

Photonic chip-based high-efficiency soliton microcombs via electrooptic-Kerr synergy

Rui Niu^{1,2,5,6,7,†}, Shuai Wan^{1,2,5,6,†}, Pi-Yu Wang^{1,2,5,6}, Rui Ma³, Jin Li^{1,2,5,6}, Fang Bo^{3,*}, Zhen Shen^{1,2,5,6}, Guang-Can Guo^{1,2,5,6}, Fang-Wen Sun^{1,2,5,6,*}, Junqiu Liu^{4,6,*}, Chun-Hua Dong^{1,2,5,6,*}

¹Laboratory of Quantum Information, University of Science and Technology of China, Hefei, Anhui 230026, China

²CAS Center For Excellence in Quantum Information and Quantum Physics,
University of Science and Technology of China, Hefei, Anhui 230088, China

³MOE Key Laboratory of Weak-Light Nonlinear Photonics,
TEDA Applied Physics Institute and School of Physics, Nankai University, Tianjin 300457, China

⁴International Quantum Academy, Shenzhen 518048, China

⁵Anhui Province Key Laboratory of Quantum Network,
University of Science and Technology of China, Hefei, Anhui 230088, China

⁶Hefei National Laboratory, University of Science and Technology of China, Hefei, Anhui 230088, China

⁷Present address: School of Physics, Harbin Institute of Technology, Harbin 150006, China and

[†]These authors contributed equally to this work.*

Temporal soliton mode-locking in coherently pumped microcavities provides a promising platform for miniaturized frequency comb systems. While significant progress has been made, achieving high conversion efficiency in such microcombs remains a critical challenge. Soliton generation through pulse pumping has emerged as an effective strategy to improve conversion efficiency. However, the on-chip integration of pulse generation with dissipative Kerr soliton (DKS) formation within the photonic chip has not yet been realized. In this work, we demonstrate a photonic chip-based soliton microcomb with high conversion efficiency, achieved by integrating on-chip pulse generation and DKS generation. The pulsed laser, fabricated on a lithium niobate-on-insulator (LNOI) platform, delivers a 35.5 GHz repetition rate with broadly tunable center frequencies. By coupling these on-chip pulses to a silicon nitride microresonator, we achieve stable DKS generation with a pump-to-soliton conversion efficiency of 43.9 % under steady-state conditions. This integrated architecture establishes a viable pathway toward chip-scale soliton microcombs with unprecedented efficiency, opening up new possibilities for optical communications, precision spectroscopy, and photonic sensing.

I. INTRODUCTION

The rapid advancement of integrated photonics has notably energized research into the generation of dissipative Kerr solitons (DKSs) on photonic chips, leveraging third-order nonlinearity within microresonators [1, 2]. DKSs offer a promising route to achieve broadband, fully coherent, chip-scale frequency combs with advantages of compact, lightweight, and energy-efficient [3, 4]. Unlike conventional mode-locked lasers, soliton microcombs operate over a wide range of repetition rates, from the microwave to the millimeter-wave domains [5, 6]. Various material platforms such as silica [7–9], silicon nitride [10, 11], silicon [12], lithium niobate [13–16], aluminum nitride [17], and silicon carbide [18, 19] have hosted demonstrations of DKS generation. The integration of photonics has played a pivotal role in enhancing the capabilities of soliton microcomb technology, significantly accelerating its adoption across various system-level applications such as telecommunications, ultrafast ranging [20–22], microwave generation [23–25], dual-comb spectroscopy [26, 27], quantum information [28], frequency synthesizers [29], and optical atomic clocks [30].

Despite their broad applicability, DKSs face several key challenges. The pump-to-soliton conversion efficiency remains relatively low, resulting in low pump energy utilization and high pump power requirements [31, 32]. Strong thermal effects in microresonators fur-

ther complicate DKS generation [33]. Moreover, stabilizing the repetition rate of DKSs requires fast photodetection and microwave signal processing, making the system more complex [34, 35].

Pulse pumping of microcavities offers a straightforward solution to these challenges. By enhancing the overlap between the pump pulse and the soliton pulse, this approach improves conversion efficiency [36, 37]. For instance, a silica microcavity pumped with pulses achieved a 34 % conversion efficiency at the steady-state [32]. Similarly, a silicon nitride-based microcomb with a detectable repetition rate of 28 GHz demonstrated an 8 % conversion efficiency and a 2/3-octave spectral span [38]. Additionally, pulse pumping mitigates thermal effects, enabling DKS generation through simple pump wavelength sweeping [32]. The repetition rate of the generated soliton is inherently locked to that of the pump pulse, thereby simplifying system design [36]. However, in the aforementioned works, the driving pulses are generated by bulky cascaded fiber-optic electro-optic modulators.

Achieving on-chip pulse-driven DKSs, where both pulse generation and DKS formation occur on the photonic chip, remains a significant challenge. A critical requirement is the precise matching of the repetition rate and center frequency of the on-chip pulse with those of the DKS. Electro-optic (EO) modulation is a well-established technique for generating optical pulses from CW lasers with tunable frequency and repetition rates

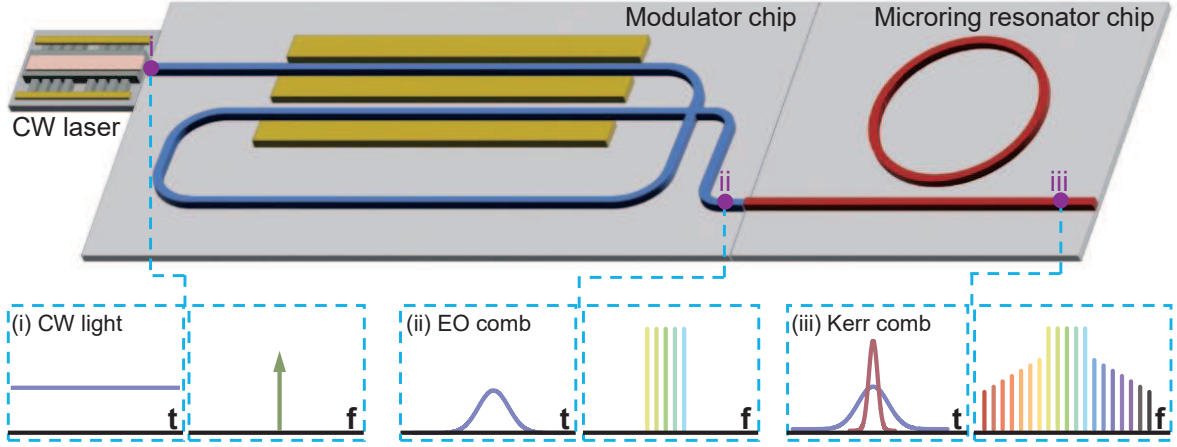


FIG. 1. The schematic of the photonic chip-based high conversion efficiency soliton microcomb. A continuous-wave is coupled into the lithium niobate photonic chip as a phase modulator for the generation of electro-optic frequency comb, which is sent to an optical microcavity to generate a DKS. The repetition rate of this electro-optic comb closely matches the FSR of the optical microcavity. Insets (i-iii) show the time domain and frequency domain of the CW light, EO comb and Kerr comb.

[39–42]. Recent advancements in the lithium niobate on insulator (LNOI) platform have enabled the generation of ultrashort on-chip pulses [43–45]. While the frequency comb generation using a $\chi^{(3)}$ resonator synchronously pumped by a tunable femtosecond pulse generator with on-chip amplitude and phase modulators has been proposed [46], the realization of combined on-chip pulse and DKS generation remains elusive.

In this paper, we present a photonic chip-based soliton microcomb with high conversion efficiency, achieved by integrating on-chip pulse generation with DKS formation. The on-chip pulses are generated on the LNOI platform with a 35.5 GHz repetition rate and a tunable center frequency, while the DKSs are generated on a silicon nitride (Si_3N_4) platform with the approximate repetition rate. Using the on-chip pulse to drive DKS generation minimizes thermal effects in the microresonator and allows for soliton formation through simple pump frequency scanning, achieving a steady-state single-soliton with conversion efficiency of 43.9%. Our work demonstrates a promising pathway toward high-efficiency, chip-scale soliton microcombs, with potential applications in optical data transmission, spectroscopy, and sensing.

II. SCHEMATIC AND DEVICE FABRICATION

The architecture of the photonic chip-based high-efficiency soliton microcomb system is illustrated in Fig. 1. This system consists of a CW laser, an on-chip phase modulator, and a microring resonator satisfying the conditions for soliton generation. The CW laser (i) is coupled into the modulator chip, where cascaded EO modulation generates an EO frequency comb. Simultaneously, the CW laser is modulated in the time domain to form a

pulsed laser (ii). The EO comb is then coupled into the microring resonator, where the center frequency and repetition rate of the comb are tuned to match the resonance modes, thereby generating a pulse-pumped soliton microcomb (iii). The insets depict the temporal and spectral characteristics at each stage of the system. Compared to conventional CW pumping schemes, the pulse-pumped approach provides higher peak power and better temporal overlap with soliton pulses. Consequently, the pump-to-comb conversion efficiency is significantly enhanced. The maximum conversion efficiency can be expressed as [32]:

$$\Gamma_{\text{pulse}} = 2\pi^2\eta^2\tau/\tau_p \quad (1)$$

where τ and τ_p represent the duration of the soliton and the pump pulse, respectively, and $\eta = Q/Q_{\text{ex}}$ represents the resonator loading factor, with Q and Q_{ex} being the total and external quality factors. According to this formula, improving the conversion efficiency requires not only maximizing the Q-factor of the microring resonator but also narrowing the pump pulse width (i.e., broadening the spectrum of the electro-optic comb).

Here, we utilized the on-chip phase modulator based on the LNOI platform to generate EO comb. For the pump temporal profile assumed here [32], we also have $\tau_p = T_R/N$, where N is the number of spectral lines in the pump, T_R is the cavity round-trip time, and where pumping close to the round-trip rate of the microcomb is assumed. In this case, the maximum efficiency can be estimated on the form

$$\Gamma_{\text{pulse}} = N\Gamma_{\text{CW}} \quad (2)$$

where Γ_{CW} is the maximum cw pumping efficiency. Ac-

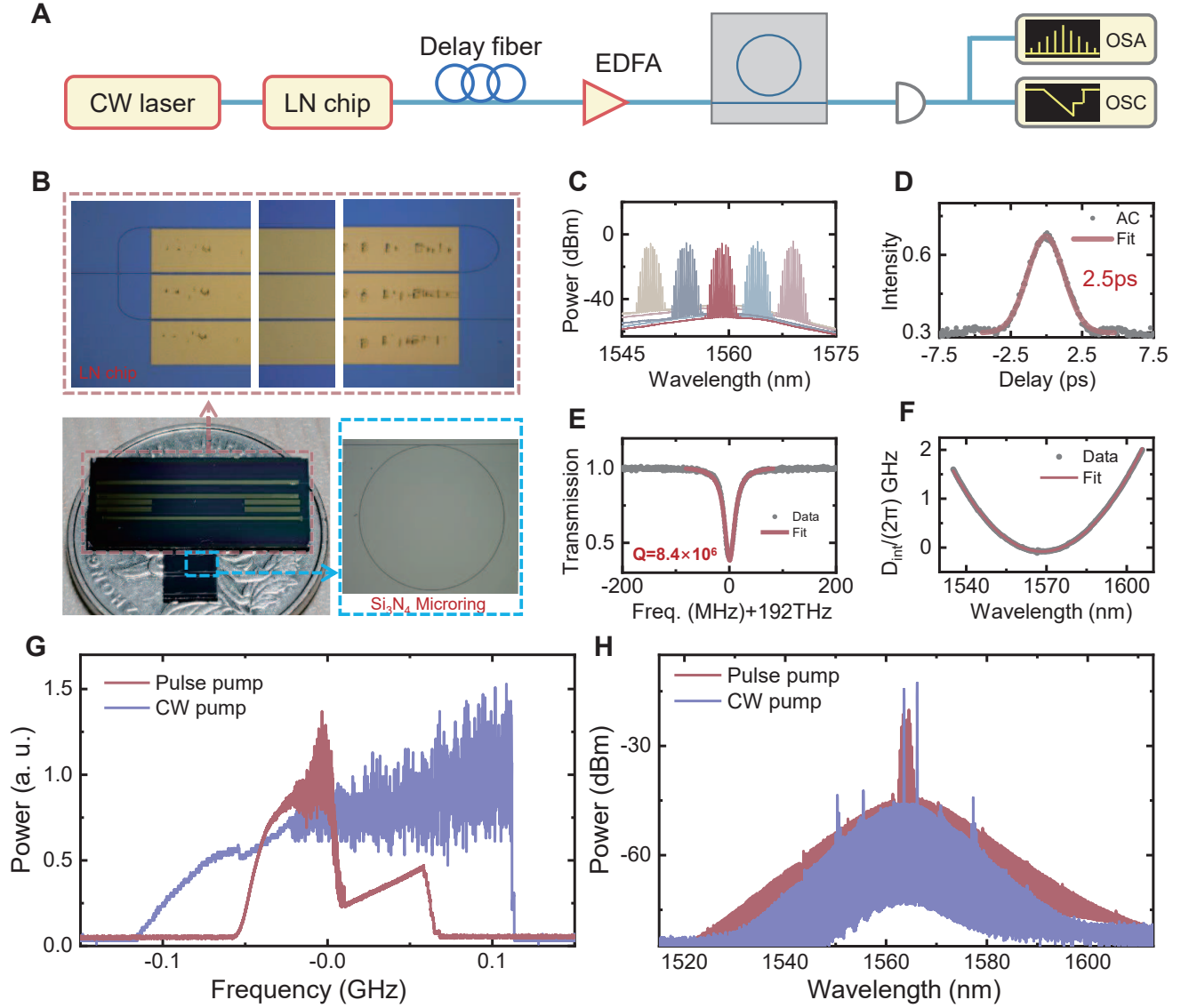


FIG. 2. (A) Schematic of the experimental setup. EDFA: erbium-doped fiber amplifier; OSC: oscilloscope; OSA: optical spectrum analyzer. (B) Photograph of the LN chip and Si_3N_4 photonic chip. The microscope image of the device consisting of a LN phase modulator with electrodes and Si_3N_4 microring resonator. (C) Optical spectrum of the EO comb before amplification with various center wavelength. (D) Autocorrelation measurement of the EO comb. (E) Resonance linewidth fitting of Si_3N_4 microring resonator, showing loaded optical Q-factor of 8.4 million. (F) The measured dispersion of the Si_3N_4 microring resonator. (G) Measured soliton step when the CW or pulse pump is scanning through the optical mode. (H) Optical spectrum of the generated DKS with the CW and pulse pump. An auxiliary laser around 1566 nm is used to compress the thermal effect with the CW pump laser.

cording to this formula, the efficiency of the pulse pumping mainly depends on the comb-line number of the EO comb. Furthermore, we generate the DKS in the microring resonator based on the Si_3N_4 platform, which offers higher Q-factors while ensuring reliable soliton microcomb generation.

The on-chip phase modulator was fabricated using a commercial x-cut LNOI wafer provided by NANOLN. This wafer consists of a 600 nm-thick x-cut LN layer, a 2 μm -thick wet-oxidized silicon dioxide (SiO_2) layer,

and a 500 μm -thick silicon substrate. Detailed fabrication processes can be found in [15]. After preparing the LN waveguides, microwave electrodes were fabricated via laser direct writing, followed by metal deposition using thermal evaporation. A dual-layer lift-off process was employed to transfer a 15 nm chromium layer and a 300 nm gold layer. The microwave electrodes are 1.9 cm long, and the LN waveguide passes through the electrodes twice to enhance the modulation efficiency.

The Si_3N_4 microresonator was fabricated using a sub-

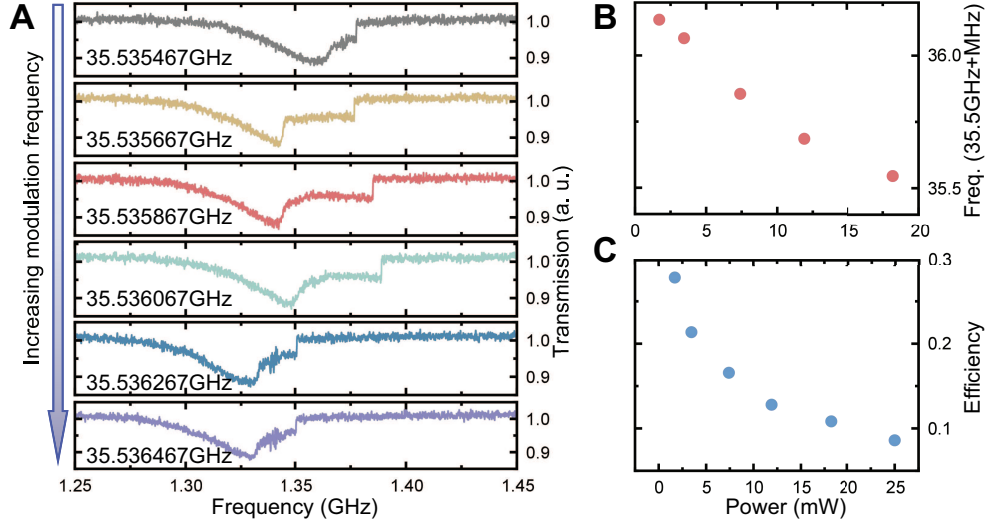


FIG. 3. (A) The transmission of the pump laser as the modulation frequency of the on-chip pulse increases from 35.535467 GHz to 35.536467 GHz. (B) Measured repetition rate versus the pump power, with the increasing of the pump power, the repetition rate decreases. (C) Measured conversion efficiency versus the pump power, with the increasing of the pump power, the conversion efficiency decreases.

tractive process [47] with 830-nm-thick Si_3N_4 on 150-mm-diameter (6-inch) wafers. The process started with deposition of 830-nm-thick Si_3N_4 on a clean thermal wet SiO_2 substrate using low-pressure chemical vapor deposition (LPCVD). Deep-ultraviolet (DUV) stepper lithography (ASML PAS850C) with 110 nm resolution was used to pattern the circuits, followed by inductively coupled plasma (ICP) etching and thermal annealing. Afterwards, Si_3N_4 annealing at 1200°C was performed to remove hydrogen content in Si_3N_4 , followed by 3- μm -thick SiO_2 top cladding deposition and another thermal annealing to eliminate hydrogen contents in SiO_2 . Finally, UV photolithography and deep dry etching were performed to define chip size and create smooth chip facets. The wafer was separated into individual chips for experiments.

III. EXPERIMENTAL RESULTS

Figure 2A illustrates the experimental setup, with the LN modulator chip and Si_3N_4 microring resonator chip shown in Fig. 2B. To achieve maximum compression of the pulsed light, the LN chip and microring resonator chip are connected by a 400-meter-long single-mode fiber. Based on the dimensions of the Si_3N_4 microring resonator, the modulation signal applied to the phase modulator is set to approximately 35.5 GHz to match the free spectral range (FSR) of the microring resonator. The spectrum of the EO comb generated after the CW laser passes through the LN chip is shown in Fig. 2C. It can be observed that the center frequency of the EO comb shifts with changes in the CW pump frequency, while the spec-

tral width remains stable at approximately 4.6 nm. The corresponding temporal pulse profile, which is obtained via autocorrelation measurements, is shown in Fig. 2D, with a pulse width of approximately 2.5 ps. The pulse is coupled into the microring resonator through the fiber lens with a coupling loss of 3.0 dB per facet. Figure 2E presents the typical resonance mode of the microring resonator, where the fitted loaded Q-factor is approximately 8.4×10^6 . Additionally, the integrated dispersion curve of the microring resonator, which is measured using a Mach-Zehnder interferometer, is shown in Fig. 2F. The results reveal anomalous dispersion near 1560 nm, with $D_2/2\pi \approx 3$ MHz.

The generation of soliton microcombs requires the pump laser to be stabilized on the soliton step on the red-detuned side of the resonance mode. However, the traditional CW pumping scheme is hindered by intracavity thermal effects, making it challenging to achieve a stable soliton state via simple wavelength scanning. Figure 2G depicts the intracavity power spectrum (purple curve) when the CW pump laser is scanned from the blue-detuned side to the red-detuned side. Only a minimal soliton step can be observed. In contrast, with pulse pumping, the improved conversion efficiency results in a pronounced soliton step in the intracavity power spectrum (red curve). This allows for stable soliton states to be achieved by simply scanning the pump laser from the blue-detuned to the red-detuned side. Figure 2H compares the soliton spectra generated by pulse pumping and CW pumping (using a dual-pumped method). Due to the significantly enhanced conversion efficiency, the soliton state generated by pulse pumping exhibits higher comb line power and broader spectral width.

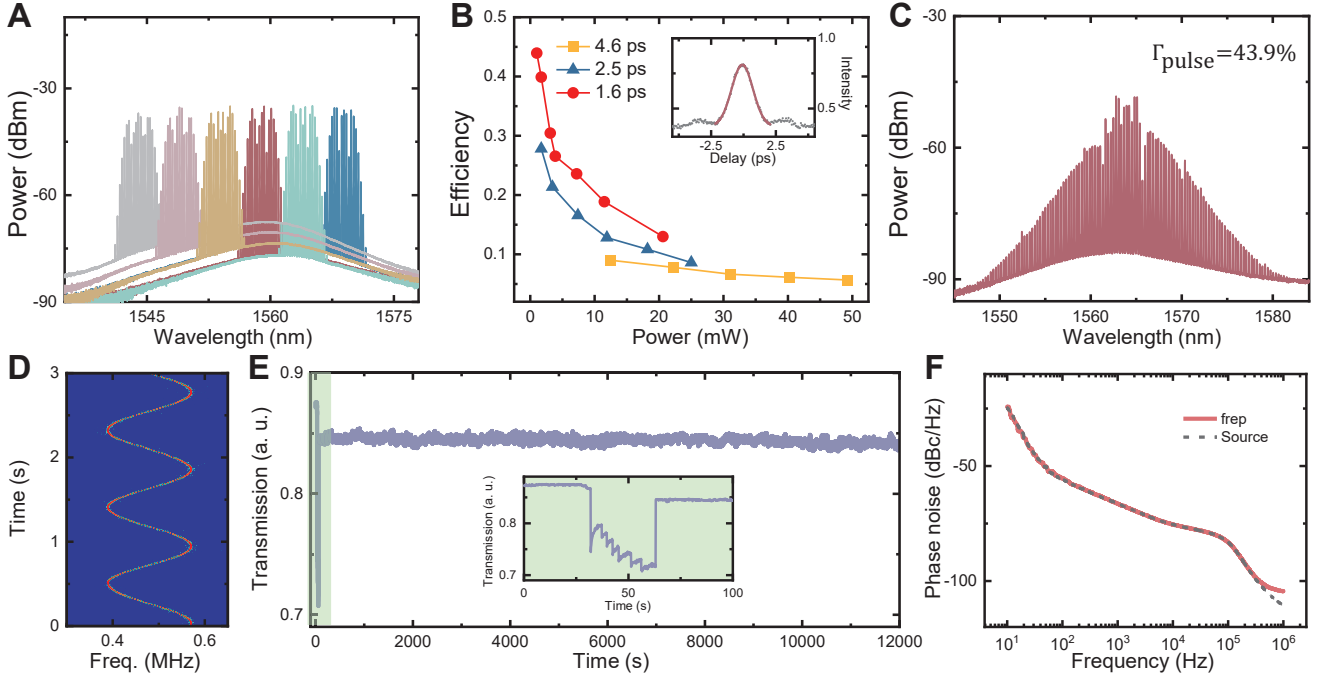


FIG. 4. **(A)** Optical spectrum of the cascaded EO comb. **(B)** The conversion efficiency of the DKSs with various pump power and different pulse width. Inset: the autocorrelation measurement of the cascaded EO comb in (A). **(C)** Optical spectrum of the DKS with the 43.9 conversion efficiency. **(D)** The real-time evolution of the repetition rate while scanning the modulation frequency. **(E)** Time-series measurements of transmission of the pump laser. **Inset:** Enlarge of the time-series measurement at 0 – 100 s. **(F)** Phase noise measurement of the repetition rate and the RF source. The phase noise of the RF source and the repetition rate are at the same level.

In the case of pulse pumping, precise matching between the modulation frequency of the phase modulator (i.e., the repetition rate of the EO comb) and the repetition rate of the soliton microcomb is critical. Figure 3A illustrates the changes in the pump laser transmission spectrum as the modulation frequency increases from 35.535467 GHz to 35.536467 GHz. As the modulation frequency increases, the matching between the modulation frequency and the soliton microcomb repetition rate improves, resulting in a broader soliton step. When the modulation frequency reaches 35.535867 GHz, the best matching is achieved, and the soliton step reaches its maximum width. Furthermore, the optimal modulation frequency is influenced by the pump power due to intracavity thermal effects. As shown in Fig. 3B, an increase in pump power leads to a reduction in the FSR of the microring resonator caused by thermal effects, which lowers the repetition rate of the soliton microcomb and, consequently, the optimal modulation frequency. Additionally, the pump laser power affects the conversion efficiency, as illustrated in Fig. 3C. The conversion efficiency decreases with increasing pump laser power. According to Eq. (2), the conversion efficiency is primarily determined by the combline number of the EO comb. While an increase in optical power does not affect these comb lines, it instead raises the total pump power. Consequently, the conver-

sion efficiency decreases as the optical power increases [48]. When the pulse width is 2.5 ps, the conversion efficiency can reach 27.8%. Here, we adopt the widely accepted definition of "conversion efficiency," which is the ratio of the power within the comb lines (excluding the power carried by the pump frequencies) to the pump laser power on chip [49]. More details of the estimation of conversion efficiency see Supplementary Information.

To further enhance the conversion efficiency, we cascaded two on-chip phase modulators to broaden the spectral width of the EO comb. After cascading, the spectral width of the EO comb is extended to 6.2 nm, with a significantly flatter spectral profile, and the corresponding pulse width is reduced to 1.6 ps, as shown in Fig. 4A. Figure 4B illustrates the variation in conversion efficiency with pump power under different pulse widths. It can be observed that, at the same pump power, narrower pulse widths result in higher conversion efficiencies, consistent with the prediction of Eq. (1). Additionally, narrower pulses provide higher peak power for the same pump power, leading to lower soliton microcomb generation thresholds. When the pulse width is reduced to 1.6 ps, a pump power as low as 1 mW is sufficient to generate a soliton microcomb, achieving a conversion efficiency of 43.9%. The corresponding soliton spectrum is shown in Fig. 4C. This power level can be easily achieved

Comb generation platform	Repetition rate (GHz)	Pump scheme	Conversion efficiency	Soliton state
SiO ₂ [32]	22.1	fiber EO comb	34%	yes
Si ₃ N ₄ [38]	27.9	fiber EO comb	8%	yes
LN[46]	30.1	on chip pulse	10%	no
our work	35.5	on chip pulse	43.9%	yes

TABLE I. Performance with other reported pulse pump high conversion efficiency Kerr combs.

with a distributed feedback (DFB) laser, making it feasible to construct fully integrated soliton microcomb with high conversion efficiency.

For quantitative characterization of repetition rate tunability, we implemented continuous sinusoidal modulation on the RF driving signal while simultaneously tracking the repetition rate shifts. The real-time measurement in Fig. 4D demonstrates a dynamic modulation range exceeding 200 kHz peak-to-peak. To fully characterize the high-conversion-efficiency DKS, it is essential to evaluate its long-term stability. We recorded the frequency variation of the pump transmission using a data acquisition card with a gate time of 0.1 s. Figure 4E shows the pump laser transmission over a period of 12000 s. At the beginning of the time series (shaded area), the pump laser frequency is manually tuned from the blue side to the red side of the cavity resonance. The enlarged time series is shown in inset of Fig. 4E. Furthermore, we also measured phase noise of the repetition rate and the RF signal using a phase noise analyzer (Rohde & Schwarz, FSWP). The results are shown in Fig. 4F, confirming that the phase noise of the RF signal and the repetition rate are at the same level.

IV. DISCUSSION

In conclusion, we have demonstrated a photonic chip-based high-efficiency soliton microcomb system that synergistically combines the exceptional EO modulation efficiency of LN with the ultralow-loss and dispersion-engineered microresonators of Si₃N₄. By modulating the CW pump source with the on-chip LN phase modulator and compressing the resulting pulses through dispersion-compensating fiber, we generate 1.6 ps optical pulses for pumping soliton microcombs. This pulse-pumping scheme achieves 43.9% conversion efficiency at an average on-chip pump power of only 1 mW, surpassing all prior pulsed microcomb systems in efficiency (Table I). Crucially, the approach reduces the soliton threshold power, suppresses thermal instabilities, and enables robust soliton generation through straightforward pump frequency scanning. These advances resolve key challenges in power efficiency and operational complexity that have hindered practical microcomb applications.

While our proof-of-concept currently employs discrete

components, recent breakthroughs in heterogeneous and hybrid photonic integration provide a clear roadmap toward full system integration. The sub-mW operational threshold enables direct driving by heterogeneous III-V DFB lasers [3], bypassing external amplifiers, as demonstrated in recent progress in laser integration on Si₃N₄ [50] and LN [51] platforms. Moreover, dispersion engineering of Si₃N₄ or LN waveguides allows on-chip pulse compression, eliminating reliance on bulk fiber components [43]. The rapid maturation of multi-material integration techniques facilitates the monolithic integration of LN modulators, Si₃N₄ dispersion compensators, and III-V pump lasers on a unified platform through III-V/Si₃N₄/LN heterogeneous bonding [52]. Such integration, leveraging fast modulation of LN and low-loss optics of Si₃N₄, establishes a scalable platform for deployable microcombs in portable sensors, optical clocks, and communication systems.

Data availability

All data needed to evaluate the conclusions in the paper are present in the paper and/or the Supplementary Information.

Acknowledgments

The work was supported by the the National Natural Science Foundation of China (12293050, 12293052, 12104442, 12304435, 12261131503, 92050109, 62225506 and 92250302), Innovation program for Quantum Science and Technology (2021ZD0303203, 2023ZD0301500), the CAS Project for Young Scientists in Basic Research (YSBR-069), the Postdoctoral Fellowship Program of CPSF (GZC20232564), the China Postdoctoral Science Foundation (2023M733414), Shenzhen Science and Technology Program (Grant No. RCJC20231211090042078), the Fundamental Research Funds for the Central Universities. This work was partially carried out at the USTC Center for Micro and Nanoscale Research and Fabrication.

Author contributions

R.N. and S.W. contribute equally to this work. R.N., S.W. and C.-H.D. conceived the experiments. S.W., P.-Y.W., R.M., J.L. and F.B. prepared devices. R.N. built the experimental setup and carried out measurements, with the assistance from F.-W.S.. R.N. and S.W. ana-

lyzed the data, with the assistance from J.L. and Z.S.. R.N., S.W., and C.-H.D. wrote the paper with input from all co-authors. C.-H.D. and G.-C.G. supervised the project. All authors contributed extensively to the work presented in this paper.

Competing financial interests

The authors declare no competing financial interests.

-
- * bofang@nankai.edu.cn, fwsun@ustc.edu.cn, liujq@iqasz.cn, chunhuan@ustc.edu.cn, liubo3@ustc.edu.cn
- [1] T. J. Kippenberg, A. L. Gaeta, M. Lipson, and M. L. Gorodetsky, “Dissipative kerr solitons in optical microresonators,” *Science* **361** (2018).
 - [2] W. Wang, L. Wang, and W. Zhang, “Advances in soliton microcomb generation,” *Advanced Photonics* **2**, 034001 (2020).
 - [3] B. Shen, L. Chang, J. Liu, H. Wang, Q.-F. Yang, C. Xiang, R. N. Wang, J. He, T. Liu, W. Xie, *et al.*, “Integrated turnkey soliton microcombs,” *Nature* **582**, 365 (2020).
 - [4] L. Chang, S. Liu, and J. E. Bowers, “Integrated optical frequency comb technologies,” *Nature Photonics* **16**, 95 (2022).
 - [5] J. Liu, E. Lucas, A. S. Raja, J. He, J. Riemensberger, R. N. Wang, M. Karpov, H. Guo, R. Bouchand, and T. J. Kippenberg, “Photonic microwave generation in the x- and k-band using integrated soliton microcombs,” *Nature Photonics* **14**, 486 (2020).
 - [6] T. Tetsumoto, T. Nagatsuma, M. E. Fermann, G. Navickaite, M. Geiselmann, and A. Rolland, “Optically referenced 300 ghz millimetre-wave oscillator,” *Nature Photonics* **15**, 516 (2021).
 - [7] Y. Bai, M. Zhang, Q. Shi, S. Ding, Y. Qin, Z. Xie, X. Jiang, and M. Xiao, “Brillouin-kerr soliton frequency combs in an optical microresonator,” *Physical Review Letters* **126**, 063901 (2021).
 - [8] L. Yao, P. Liu, H.-J. Chen, Q. Gong, Q.-F. Yang, and Y.-F. Xiao, “Soliton microwave oscillators using oversized billion q optical microresonators,” *Optica* **9**, 561 (2022).
 - [9] R. Niu, M. Li, S. Wan, Y. R. Sun, S.-M. Hu, C.-L. Zou, G.-C. Guo, and C.-H. Dong, “khz-precision wavemeter based on reconfigurable microsoliton,” *Nature Communications* **14**, 169 (2023).
 - [10] A. Rao, G. Moille, X. Lu, D. A. Westly, D. Sacchetto, M. Geiselmann, M. Zervas, S. B. Papp, J. Bowers, and K. Srinivasan, “Towards integrated photonic interposers for processing octave-spanning microresonator frequency combs,” *Light: Science & Applications* **10**, 109 (2021).
 - [11] G. Moille, J. Stone, M. Chojnacky, R. Shrestha, U. A. Javid, C. Menyuk, and K. Srinivasan, “Kerr-induced synchronization of a cavity soliton to an optical reference,” *Nature* **624**, 267 (2023).
 - [12] M. Yu, Y. Okawachi, A. G. Griffith, N. Picqué, M. Lipson, and A. L. Gaeta, “Silicon-chip-based mid-infrared dual-comb spectroscopy,” *Nature Communications* **9**, 1869 (2018).
 - [13] Y. He, R. Lopez-Rios, U. A. Javid, J. Ling, M. Li, S. Xue, K. Vahala, and Q. Lin, “High-speed tunable microwave-rate soliton microcomb,” *Nature Communications* **14**, 3467 (2023).
 - [14] C. Yang, S. Yang, F. Du, X. Zeng, B. Wang, Z. Yang, Q. Luo, R. Ma, R. Zhang, D. Jia, *et al.*, “1550-nm band soliton microcombs in ytterbium-doped lithium-niobate microrings,” *Laser & Photonics Reviews* **17**, 2200510 (2023).
 - [15] S. Wan, P.-Y. Wang, R. Ma, Z.-Y. Wang, R. Niu, D.-Y. He, G.-C. Guo, F. Bo, J. Liu, and C.-H. Dong, “Photorefraction-assisted self-emergence of dissipative kerr solitons,” *Laser & Photonics Reviews* **18**, 2300627 (2024).
 - [16] X. Lv, B. Nie, C. Yang, R. Ma, Z. Wang, Y. Liu, X. Jin, K. Zhu, Z. Chen, D. Qian, *et al.*, “Broadband microwave-rate dark pulse microcombs in dissipation-engineered linbo3 microresonators,” *Nature Communications* **16**, 2389 (2025).
 - [17] A. W. Bruch, X. Liu, Z. Gong, J. B. Surya, M. Li, C.-L. Zou, and H. X. Tang, “Pockels soliton microcomb,” *Nature Photonics* **15**, 21 (2021).
 - [18] C. Wang, J. Li, A. Yi, Z. Fang, L. Zhou, Z. Wang, R. Niu, Y. Chen, J. Zhang, Y. Cheng, *et al.*, “Soliton formation and spectral translation into visible on cmos-compatible 4h-silicon-carbide-on-insulator platform,” *Light: Science & Applications* **11**, 341 (2022).
 - [19] M. A. Guidry, D. M. Lukin, K. Y. Yang, R. Trivedi, and J. Vučković, “Quantum optics of soliton microcombs,” *Nature Photonics* **16**, 52 (2022).
 - [20] R. Chen, H. Shu, B. Shen, L. Chang, W. Xie, W. Liao, Z. Tao, J. E. Bowers, and X. Wang, “Breaking the temporal and frequency congestion of lidar by parallel chaos,” *Nature Photonics* **17**, 306 (2023).
 - [21] B. Shi, Y.-H. Luo, W. Sun, Y. Hu, J. Long, X. Bai, A. Wang, and J. Liu, “Frequency-comb-linearized, widely tunable lasers for coherent ranging,” *Photonics Research* **12**, 663 (2024).
 - [22] S. Zhu, Y. Zhang, J. Feng, Y. Wang, K. Zhai, H. Feng, E. Y. B. Pun, N. H. Zhu, and C. Wang, “Integrated lithium niobate photonic millimetre-wave radar,” *Nature Photonics* **19**, 204 (2025).
 - [23] S. Sun, B. Wang, K. Liu, M. W. Harrington, F. Tabatabaei, R. Liu, J. Wang, S. Hanifi, J. S. Morgan, M. Jahanbozorgi, *et al.*, “Integrated optical frequency division for microwave and mmwave generation,” *Nature* **627**, 540 (2024).
 - [24] R. Niu, T.-P. Hua, Z. Shen, Y. Wang, S. Wan, Y. R. Sun, W. Wang, W. Zhao, G.-C. Guo, W. Zhang, *et al.*, “Ultralow-noise k-band soliton microwave oscillator using optical frequency division,” *ACS Photonics* **11**, 1412 (2024).
 - [25] Y. Zhao, J. K. Jang, G. J. Beals, K. J. McNulty, X. Ji, Y. Okawachi, M. Lipson, and A. L. Gaeta, “All-optical frequency division on-chip using a single laser,” *Nature* **627**, 546 (2024).
 - [26] C. Bao, Z. Yuan, L. Wu, M.-G. Suh, H. Wang, Q. Lin, and K. J. Vahala, “Architecture for microcomb-based ghz-mid-infrared dual-comb spectroscopy,” *Nature Communications* **12**, 6573 (2021).
 - [27] J.-T. Li, B. Chang, J.-T. Du, T. Tan, Y. Geng, H. Zhou, Y.-P. Liang, H. Zhang, G.-F. Yan, L.-M. Ma, *et al.*, “Coherently parallel fiber-optic distributed acoustic sensing using dual kerr soliton microcombs,” *Science Advances* **10**, eadf8666 (2024).
 - [28] L. Huang, W. Wang, F. Wang, Y. Wang, C. Zou, L. Tang,

- B. E. Little, W. Zhao, Z. Han, J. Yang, *et al.*, “Massively parallel hong-ou-mandel interference based on independent soliton microcombs,” *Science Advances* **11**, eadq8982 (2025).
- [29] D. T. Spencer, T. Drake, T. C. Briles, J. Stone, L. C. Sinclair, C. Fredrick, Q. Li, D. Westly, B. R. Ilic, A. Bluestone, *et al.*, “An optical-frequency synthesizer using integrated photonics,” *Nature* **557**, 81 (2018).
- [30] K. Wu, N. P. O’Malley, S. Fatema, C. Wang, M. Girardi, M. S. Alshaykh, Z. Ye, D. E. Leaird, M. Qi, V. Torres-Company, *et al.*, “Vernier microcombs for integrated optical atomic clocks,” *Nature Photonics* **19**, 400 (2025).
- [31] Ó. B. Helgason, F. R. Arteaga-Sierra, Z. Ye, K. Twayana, P. A. Andrekson, M. Karlsson, and J. Schröder, “Dissipative solitons in photonic molecules,” *Nature Photonics* **15**, 305 (2021).
- [32] J. Li, C. Bao, Q.-X. Ji, H. Wang, L. Wu, S. Leifer, C. Beichman, and K. Vahala, “Efficiency of pulse pumped soliton microcombs,” *Optica* **9**, 231 (2022).
- [33] S. Zhang, J. M. Silver, L. Del Bino, F. Copie, M. T. Woodley, G. N. Ghalanos, A. Ø. Svela, N. Moroney, and P. Del’Haye, “Sub-milliwatt-level microresonator solitons with extended access range using an auxiliary laser,” *Optica* **6**, 206 (2019).
- [34] Z. L. Newman, V. Maurice, T. Drake, J. R. Stone, T. C. Briles, D. T. Spencer, C. Fredrick, Q. Li, D. Westly, B. R. Ilic, *et al.*, “Architecture for the photonic integration of an optical atomic clock,” *Optica* **6**, 680 (2019).
- [35] T. E. Drake, T. C. Briles, J. R. Stone, D. T. Spencer, D. R. Carlson, D. D. Hickstein, Q. Li, D. Westly, K. Srinivasan, S. A. Diddams, *et al.*, “Terahertz-rate kerr-microresonator optical clockwork,” *Physical Review X* **9**, 031023 (2019).
- [36] E. Obrzud, S. Lecomte, and T. Herr, “Temporal solitons in microresonators driven by optical pulses,” *Nature Photonics* **11**, 600 (2017).
- [37] C. Zhang, R. Miao, K. Yin, X. Cheng, and T. Jiang, “Impact of pulse chirp and desynchronization on chip-based pulse-driven soliton microcombs,” *ACS Photonics* **12**, 1609 (2025).
- [38] M. H. Anderson, R. Bouchand, J. Liu, W. Weng, E. Obrzud, T. Herr, and T. J. Kippenberg, “Photonic chip-based resonant supercontinuum via pulse-driven kerr microresonator solitons,” *Optica* **8**, 771 (2021).
- [39] K. Beha, D. C. Cole, P. Del’Haye, A. Coillet, S. A. Diddams, and S. B. Papp, “Electronic synthesis of light,” *Optica* **4**, 406 (2017).
- [40] Y. Qi and Y. Li, “Integrated lithium niobate photonics,” *Nanophotonics* **9**, 1287 (2020).
- [41] R. Zhuang, K. Ni, G. Wu, T. Hao, L. Lu, Y. Li, and Q. Zhou, “Electro-optic frequency combs: Theory, characteristics, and applications,” *Laser & Photonics Reviews* **17**, 2200353 (2023).
- [42] R. Niu, S. Wan, W. Li, P.-Y. Wang, F.-W. Sun, F. Bo, J. Liu, G.-C. Guo, and C.-H. Dong, “An integrated wavemeter based on fully-stabilized resonant electro-optic frequency comb,” *Communications Physics* **6**, 329 (2023).
- [43] M. Yu, D. Barton III, R. Cheng, C. Reimer, P. Kharel, L. He, L. Shao, D. Zhu, Y. Hu, H. R. Grant, *et al.*, “Integrated femtosecond pulse generator on thin-film lithium niobate,” *Nature* **612**, 252 (2022).
- [44] K. Zhang, W. Sun, Y. Chen, H. Feng, Y. Zhang, Z. Chen, and C. Wang, “A power-efficient integrated lithium niobate electro-optic comb generator,” *Communications Physics* **6**, 17 (2023).
- [45] Q. Guo, B. K. Gutierrez, R. Sekine, R. M. Gray, J. A. Williams, L. Ledezma, L. Costa, A. Roy, S. Zhou, M. Liu, *et al.*, “Ultrafast mode-locked laser in nanophotonic lithium niobate,” *Science* **382**, 708 (2023).
- [46] R. Cheng, M. Yu, A. Shams-Ansari, Y. Hu, C. Reimer, M. Zhang, and M. Lončar, “Frequency comb generation via synchronous pumped χ (3) resonator on thin-film lithium niobate,” *Nature Communications* **15**, 3921 (2024).
- [47] Z. Ye, H. Jia, Z. Huang, C. Shen, J. Long, B. Shi, Y.-H. Luo, L. Gao, W. Sun, H. Guo, *et al.*, “Foundry manufacturing of tight-confinement, dispersion-engineered, ultralow-loss silicon nitride photonic integrated circuits,” *Photonics Research* **11**, 558 (2023).
- [48] M. Li, X.-X. Xue, Y.-L. Zhang, X.-B. Xu, C.-H. Dong, G.-C. Guo, and C.-L. Zou, “Breaking the efficiency limitations of dissipative kerr solitons using nonlinear couplers,” *Science China Physics, Mechanics & Astronomy* **67**, 234211 (2024).
- [49] Q.-F. Yang, Y. Hu, V. Torres-Company, and K. Vahala, “Efficient microresonator frequency combs,” *eLight* **4**, 18 (2024).
- [50] C. Xiang, J. Liu, J. Guo, L. Chang, R. N. Wang, W. Weng, J. Peters, W. Xie, Z. Zhang, J. Riemensberger, *et al.*, “Laser soliton microcombs heterogeneously integrated on silicon,” *Science* **373**, 99 (2021).
- [51] M. Li, L. Chang, L. Wu, J. Staffa, J. Ling, U. A. Javid, S. Xue, Y. He, R. Lopez-Rios, T. J. Morin, *et al.*, “Integrated poekels laser,” *Nature Communications* **13**, 5344 (2022).
- [52] M. Churaev, R. N. Wang, A. Riedhauser, V. Snigirev, T. Blésin, C. Möhl, M. H. Anderson, A. Siddharth, Y. Popoff, U. Drechsler, *et al.*, “A heterogeneously integrated lithium niobate-on-silicon nitride photonic platform,” *Nature Communications* **14**, 3499 (2023).